# IMPACT OF A LOSSY IMAGE COMPRESSION ON PARAMETER ESTIMATION WITH PERIODIC ACTIVE THERMAL IMAGING

Agnès Delahaies[1], David Rousseau[1], Laetitia Perez[2]
Laurent Autrique[1] and François Chapeau-Blondeau[1]
[1]*Laboratoire d'Ingénierie des Systèmes Automatisés (LISA), Université d'Angers*
*62 avenue Notre Dame du Lac, 49000 Angers, France*
[2]*Laboratoire de Thermocinétique de Nantes, Rue Christian Pauc, 44000 Nantes, France*

Keywords: Image compression, Thermal imaging, Parameter estimation, Material characterization.

Abstract: Periodic thermal imaging is a method of active thermography based on a periodic thermal stimulation of an inspected sample material and the analysis of its thermal response when a steady regime is reached. The original data, a sequence of images sampling the thermal response on a large number of periods, are usually stored in a raw format. For accurate exploitation of these measurements, the whole sequence of images requires a significant amount of storage space. In this report, we address the question of the lossy compression of these sequences of images when they are applied to perform physical parameter estimation. The study investigates the impact of lossy image compression on the performance of the physical parameter estimation procedure, and shows the possibility of preserving robust estimation with high compression rate. Perspectives and applications are then discussed. Performing good enough estimate of physical parameters with compressed images would permit the use of portable thermal cameras with limited resources in terms of data storage. This would enable the use of periodic active thermal imaging to perform relatively low cost embedded characterization of thermal properties of materials.

## 1 INTRODUCTION

Recent advances (technological improvement, or reduction of the production costs) in the domain of photonic devices, imaging sensors, involving data acquisition, transmission and storage, constitute a stimulating source of research for information sciences. Recently, there has been the emergence of new types of nonconventional imaging (polarimetric imaging, multi-or hyperspectral imaging, ...) which used to be limited by their capacity of acquisition and storage of information. Novel domains of application, formerly restricted by the production costs, have also appeared for existing imaging systems (MRI or thermal imaging). This context brings forth new configurations and challenges for the classical signal and image processing operations (detection, estimation, segmentation, compression, ...).

In this framework, we consider here a task of compression applied to thermal imaging. Introduced in the 1960's, thermal imaging uses the Planck law (Lugin, 2008; Breitenstein et al., 2003) which expresses the luminance of a black body in thermal equilibrium at a given wavelength to measure temperatures. Thermal images poses a practical problem in terms of compression when long sequences of images are required. This is specially the case with active thermography methods where the thermal evolution of a scene is recorded while some external time varying energy is injected into the scene. There are two main distinct techniques of active thermal imaging : pulsed thermal imaging (Lugin, 2008) and periodic thermal imaging (Breitenstein et al., 2003). The question of compression has only recently (Lugin, 2008) received some attention in the domain of active pulsed thermal imaging. In this report we consider periodic thermal imaging which, to the best of our knowledge, has not been yet considered under the scope of compression. We investigate the impact of a lossy compression on the performance of a parameter estimation with periodic thermal imaging.

Delahaies A., Rousseau D., Perez L., Autrique L. and Chapeau-Blondeau F. (2010).
IMPACT OF A LOSSY IMAGE COMPRESSION ON PARAMETER ESTIMATION WITH PERIODIC ACTIVE THERMAL IMAGING.
In *Proceedings of the International Conference on Imaging Theory and Applications and International Conference on Information Visualization Theory and Applications*, pages 17-22
DOI: 10.5220/0002816500170022

## 2 PRINCIPLE OF PERIODIC ACTIVE THERMAL IMAGING

The principe of periodic active thermal imaging is depicted in Fig. 1. The setup of Fig. 1 describes the inspection of a material sample $\Omega$ a solid of thickness $e$. We note $X = (x,y,z)$. The front surface $(\Gamma_0 : X_0 = (x,y,0) \in \Omega)$ of the sample $\Omega$ receives a sinusodal radiative flux with angular frequency $\omega$. The radiative flux $\Phi : \Phi_0 \cos(\omega t)$ is spatially centered on $O = (0,0,0)$ and is uniform over a disk of radius $R$ and zero outside this disk. If the radiative flux is absorbed by the material, the resulting heat diffuses inside the material. When the diffused heat arrives on the opposite side $(\Gamma_e : X_e = (x,y,e) \in \Omega)$ a flux is radiated. A thermal imaging camera is placed on the opposite side to the incident radiative flux source and receives a transmitted radiative flux.

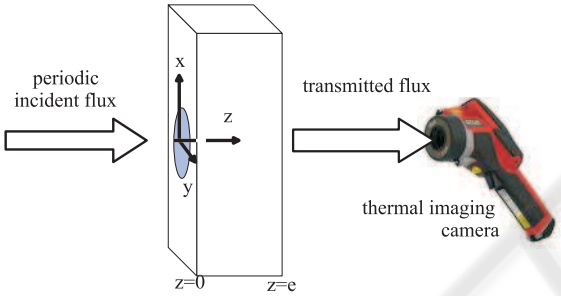


Figure 1: Principe of periodic active thermal imaging for the inspection of a material sample $\Omega$ of thickness $e$.

The camera then uses the Planck law to calculate the surface temperature on $\Gamma_e$ from this transmitted radiative flux. When the steady periodic regime is reached, the temperature in the sample $\Omega$ and on the opposite side $\Gamma_e$ is $\theta(X,t) = \mathcal{R}e\{\underline{\theta}(X,t)\}$ (Breitenstein et al., 2003) with

$$\underline{\theta}(X,t) = \theta_{DC}(X) + M(X)\exp(j\omega t)\exp(j\varphi(X)) \,, \tag{1}$$

where $\theta_{DC}(X)$ is the average temperature at $X$, $M(X)$ is the modulus image of the thermal oscillations which depicts the spatial attenuation of the incident heat flux in the material sample, and $\varphi(X)$ the phase image which represents the delay between the incident and the transmitted heat flux due to the material sample. Both images $M(X)$ and $\varphi(X)$ thus carry information on the thermal properties of the material. A specific interest of the phase $\varphi(X)$ is that it does not depend on the knowledge of the sample emissivity (Breitenstein et al., 2003). In the following we will thus only use the phase $\varphi(X)$ to analyze the thermal behavior of the sample.

There are various experimental sources of noise in the phase image $\varphi(X)$ including spurious high frequency components in the excitation and electronic noise on the thermal cameras. Therefore, high accuracy measurement of $\varphi(X)$ requires heavy statistics. A sequence of $N$ thermal images $\theta(X,n)$ with $n \in [0, N-1]$ is usually acquired to cover a large number of periods $\frac{2\pi}{\omega}$ with a high frequency rate (typically of some 50 images per period). If we assume the noise in $\theta(X,n)$ to be Gaussian, the maximum likelihood estimator $\hat{\varphi}(X)$ of image $\varphi(X)$ can be shown to be approximately for large $N$ (Kay, 1993)

$$\hat{\varphi}(X) = \arctan\left(-\frac{\beta_2(X)}{\beta_1(X)}\right) \,, \tag{2}$$

with

$$\beta_1(X) = \frac{2}{N}\sum_{n=0}^{N-1} \theta(X,n)\cos\left(\omega\frac{n}{F_e}\right) \,, \tag{3}$$

and

$$\beta_2(X) = \frac{2}{N}\sum_{n=0}^{N-1} \theta(X,n)\sin\left(\omega\frac{n}{F_e}\right) \,. \tag{4}$$

An example of phase $\hat{\varphi}(X)$ evaluated from the experimental setup of Fig. 2 is visible in Fig. 3. As explained in Fig. 2, the amount of memory required to produce Fig. 3 with a good accuracy is huge.

In the following, we are going to show how it is possible to use the phase images $\varphi(X)$ of Fig. 3 to perform estimation of a physical parameter in a material. We will then compare the performance of this estimate with a periodic active thermal imaging sequence applied on raw thermal images $\theta(X,n)$ and on the same sequence after a lossy compression.

## 3 APPLICATION TO PARAMETER ESTIMATION

Periodic active thermal imaging as described in section 2 can be applied to perform physical parameter estimation of a material. This requires the modeling of the sample response of Fig. 2 which can be done in the following way (Perez and Autrique, 2009). Temperature $\theta(X,t)$ in the material sample $\Omega$, assumed here homogeneous and isotropic, follows from heat diffusion equation

$$\alpha\frac{\partial\theta(X,t)}{\partial t} - \Delta\theta(X,t) = 0 \,, \forall (X,t) \in \Omega \times T \,, \tag{5}$$

and boundary conditions on $\Gamma_0$

$$\lambda\frac{\partial\theta(X,t)}{\partial z} = h\theta(X,t) - \Phi \,, \forall (X,t) \in \Gamma_0 \times T \,, \tag{6}$$

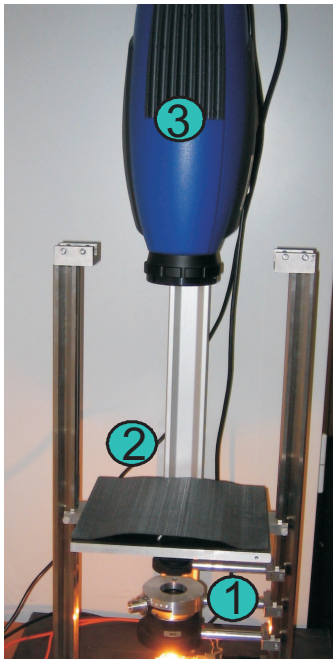


Figure 2: Experimental setup of periodic active thermal imaging used to perform the analysis. The material sample (sticker 2) taken as reference is a plate of titanium of thichness $e = 1$ mm. This sample is placed in the focal plane of a Köhler lightning device (sticker 1) which produces a uniform flux on a circular disk of radius $R = 2.5$ mm. The incident radiative flux is produced by an halogen lamp (36V-400W) placed under the sample and controlled by a on/off switch of angular frequency $\omega = 5.66$ rad.$s^{-1}$. Thermal images $\theta(X,n)$ are acquired by a SC5000 FLIR thermal camera (sticker 3) at the sampling frequency $F_e = 50$ Hz with format $320 \times 256$ coded on 14 bits. The phenomenon is recorded on 18 periods. This produce a file of 999 images representing **1.67 Go** to be stored.

on $\Gamma_e$

$$\lambda \frac{\partial \theta(X,t)}{\partial z} = h\theta(X,t) \ , \forall (X,t) \in \Gamma_e \times T \ , \qquad (7)$$

and initial temporal condition $\theta(X,0) = 0 \ \forall (X) \in \Omega$. Physical parameters of the modeling of Eqs. (5)-(7) are the diffusivity $\alpha$ in $[m^2.s^{-1}]$, the convective coefficient $h$ in $[W.m^{-2}.K^{-1}]$ and the conductivity $\lambda = \alpha\rho c$ in $[W.m^{-1}.K^{-1}]$ where $\rho$ is the density in $[kg.m^{-3}]$ and $c$ the specific heat in $[J.kg^{-1}.K^{-1}]$. Resolution of Eqs. (5)-(7) provides the temperature $\theta(X,t)$ in the whole material $\Omega$. It is then possible to confront the temperature $\theta(X,t)$ on the surface of the side $\Gamma_e$ measured by the thermal imaging and deduced by the model of Eqs. (5)-(7). One can use this experiment-model confrontation to estimate the value of an unknown parameter. In the general case, there exists no exact analytical explicit expressions for $\varphi(X)$. The solution of Eqs. (5)-(7) can be numerically performed

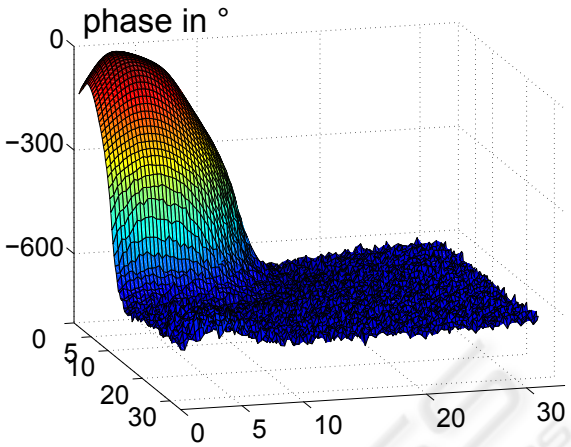


Figure 3: Phase $\varphi(X)$ evaluated with Eqs. (2)-(4) from raw images acquired with experimental setup and material sample described in Fig. 2. The phase plotted as a function of position (x,y) in mm has been unwrapped with the standard Itoh's algorithm (Ghiglia and Pritt, 1998).

by the method of (Perez and Autrique, 2009). We show in Fig. 4 an example of confrontation of an experimental phase $\varphi(X)$ obtained with the setup of Fig. 1 and the algorithm of Eqs. (2)-(4) with the numerical resolution of Eqs. (5)-(7). In Fig. 4, the unknown parameter is the conductivity $\lambda$. The estimated value (given in Table 1 for the material of Fig. 2) is chosen as the one which minimizes the average quadratic error between the phase $\varphi(X)$ in experiments and in the numerical solution of Eqs. (5)-(7).

In Fig. 4, the parameter estimation has been performed on raw data. We will now compare with the estimation when the algorithm of Eqs. (2)-(4) is performed on compressed images.

## 4 INFLUENCE OF A LOSSY COMPRESSION

To illustrate our methodology in assessing the impact of a lossy compression of images on physical parameters estimation, we choose one lossy compression technique usually implemented by default in thermal cameras. A reasonable choice (Bovik, 2000) is the standard JPEG compression. Temperature images $\theta(X,n)$ are coded on 14 bits with the camera presented in Fig. 2. The standard JPEG compression codes images on 8 bits. Therefore, requantization (already bringing a $2^{14}/2^8$ compression factor) and normalization are necessary before the JPEG compression step is applied. For each image $\theta(X,n)$ of the acquired sequence, the maximum $\theta_{max}$ and minimum $\theta_{min}$ temperature over the whole sequence are stored separately and an intermediate 8-bit gray level image

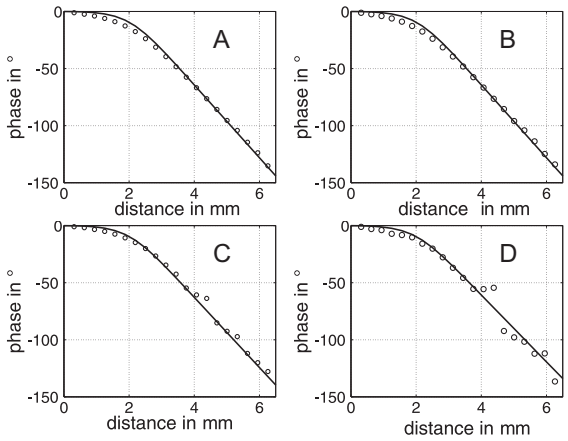


Figure 4: Phase as a function of distance. Solid line is the numerical solution of Eqs. (5)-(7) with $\alpha = 9.3 \times 10^{-6} m^2.s^{-1}$, $h = 20\ W.m^{-2}.K^{-1}$, $\rho = 4507\ kg.m^{-3}$, $c = 520\ J.kg^{-1}.K^{-1}$. Circles stand for the experimental points obtained from the setup of Fig. 2. By comparison with Fig. 3, the analysis is performed on a line starting at the maximum heating point in the modulus image $M(X,t)$ taken as phase reference. (A) is for a phase calculated with raw images directly acquired by the thermal camera. (B)(C)(D) is for a phase calculated with images after a JPEG compression with compression parameter CMP of section 4 respectively equal to 100, 90 and 25. The conductivity estimated from each panel (A)-(D) are visible in Table 1.

$I(X,n)$ is created with

$$I(X,n) = \frac{255}{\theta_{max} - \theta_{min}} (\theta(X,n) - \theta_{min}) \ . \qquad (8)$$

A standard JPEG compression is then applied to $I(X,n)$ to create the compressed sequence of images $I_{CMP}(X,n)$. We used the JPEG compression available in the programming language Matlab (version 7) with a compression parameter CMP in the range [1-100] for varying the quality/size ratio. The value 100 for CMP corresponds to high quality at low compression and 1 to low quality at high compression. A visual appreciation of the typical impact of the distorsion due to this JPEG compression is visible in Fig. 5. For an uncompressed raw image $I(X,n)$ in Fig. 5A considered at a given instant $n$, Fig. 5 displays, for various values of the compression parameter CMP, the error image $\varepsilon(X,n)$ defined as

$$\varepsilon(X,n) = I(X,n) - I_{CMP}(X,n) \ . \qquad (9)$$

A possible way to quantify the distorsion due to the lossy compression is to calculate a spatial mean square error for each sample $n$

$$MSE(n) = \langle \varepsilon(X,n) \rangle_X \ . \qquad (10)$$

Temporal evolutions of MSE of Eq. (10) are given in Fig. 6.

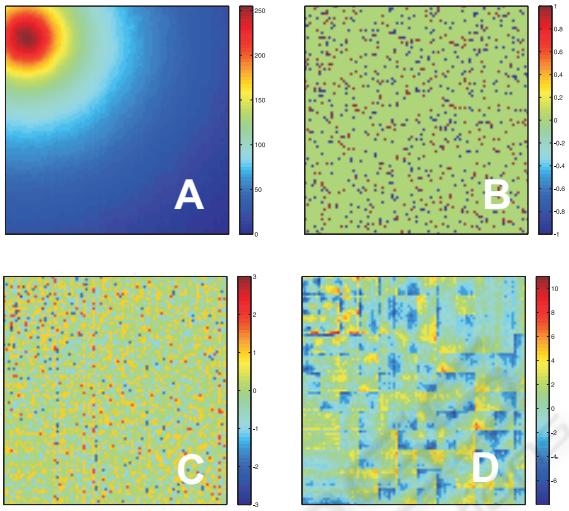


Figure 5: Panel A : uncompressed raw image $I(X,n)$ of temperature coded on 256 digital levels according to Eq. (8). Panels (B,C,D) : error images $\varepsilon(X,n)$ of Eq. 9 for decreasing compression parameter CMP respectively equal to 100, 90, 25 and corresponding compression rates indicated in Table 1.

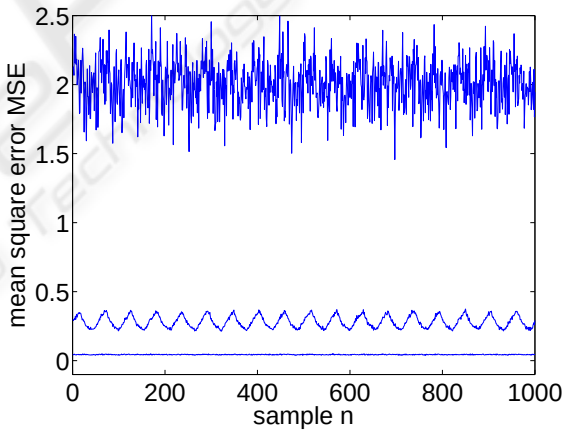


Figure 6: Mean square error MSE of Eq. (10) temporal evolutions along the 999 images acquired with the setup of Fig. 2 after JPEG compression. From bottom to up the compression parameter CMP is respectively equal to 100, 90, 25.

It is possible from Fig. 5 and Fig. 6 to figurate how both spatial and temporal noise will disturb the image sequence. However, distorsion measured by the mean square error does not assess the impact of the compression on the useful information carried by the sequence concerning the parameter to be estimated. This type of questioning also arises when the perceived distorsion due to a lossy compression is appreciated by the human vision. Psychovisual experiments are requested in this case. Here, since we are in a measurement context, we can objectively address

the quantitative impact of the distorsion on the quality of the measure. To this end, we now perform the parameter estimation procedure of section 3 on the sequence of images $I_{CMP}(X,n)$ for several values of the compression rate controlled by the compression parameter CMP. The results, visible in Table 1, show how the quality of the estimate is affected by the lossy compression. The CMP coefficient acts on the size of the imagette used to perform the JPG compression. For low values of parameter CMP (in Fig. 4D) some discontinuities due to these imagette are clearly visible. Nevertheless, thermal images $\theta(X,n)$ are varying very smoothly in the spatial domain. JPEG algorithm acts like a low-pass filter for spatial frequencies which tends to preserve the low frequencies of $\theta(X,n)$. Therefore, it appears that for sufficiently low (up to 66%) compression rate the compression distortion on each individual image barely has no effect on the useful information carried by the whole sequence. As demonstrated in Table 1, the estimation error by comparison with raw datas increases slower than the compression rate decreases. The measurement allows to perform identification of the class of material in terms of thermal properties even at very high compression rate.

Table 1: Estimate of the conductivity $\lambda$ of the material sample of Fig. 2 in $[W.m^{-1}.K^{-1}]$ performed after lossy JPEG compression at various rate ($CR = size(I_{CMP}(X,n))/size(\theta(X,n))$. As a comparison, the typical $\lambda$ for titanium is expected in the range 5 to 25 $W.m^{-1}.K^{-1}$ depending on the purity of the material. As an order of magnitude thermal conductivity of pure copper is 401 $W.m^{-1}.K^{-1}$ and pure aluminium is 237 $W.m^{-1}.K^{-1}$

| CR | CMP | estimate | relative error |
|---|---|---|---|
| raw | | 21.42 | 0 % |
| 66% | 100 | 21.41 | 0.04% |
| 88% | 90 | 23.24 | 8.54% |
| 94% | 25 | 25.88 | 20.8% |

# 5 CONCLUSIONS

In this report we have shown and analyzed quantitatively the robustness of parameter estimation with periodic active thermal imaging toward lossy JPEG compression. An originality in our approach by comparison with the recent work of (Lugin, 2008) is that we have not considered the distortion due to lossy image compression on the thermal images but directly on the quantitative information they carry. This approach is interesting in general for quantitative physical imaging since it shows the possibility of conditions where lossy image compression can entail almost no loss in the information extracted form the image.

Further development of this work is to consider video-compression algorithms (Shi and Sun, 2000) to compress the whole sequence of images. Instead of compressing each image separately, video-compression treats groups of successive pictures. This video compression would enable higher compression rates and bring additional distortion on the information carried on each pixel with time. Other ways to reduce the amount of data required by periodic active thermal imaging are also to decrease the sampling frequency, the imaging sensor dynamic and the number of pixels. It would then be interesting to see how these configurations together with video lossy compression degrade the quality of the estimate of physical parameters. For illustration in this report, the unknown parameter to be estimated was the conductivity. The sensitivity to compression distorsion could also depend on the parameter to be estimated and it would also be important to explore this systematically while investigating other compression schemes.

Typical limit to look for in terms of compression would be in the direction of the technical characteristics of the new portable thermal cameras which are now available at relative low cost. An MPEG video flux is usually available as an output of these cameras. This facility is initially thought as a qualitative tool enabling the display of thermal images on screens larger than the screen of the camera itself. Yet, as illustrated in this report, periodic active thermal imaging only requires the relative spatial and temporal variations of the gray levels to perform quantitative measurement. An application of our results would therefore be to evaluate the possible usefulness of these portable thermal cameras for quantitative periodic active thermal imaging.

# ACKNOWLEDGEMENTS

Authors would like to thank Patrice BALCON and Franck CARETTE from FLIR Systems for useful discussions.

# REFERENCES

Bovik, A. C. (2000). *Handbook of Image and Video Processing*. Academic Press, New York.

Breitenstein, O., Warta, W., and Langenkamp, M. (2003). *Lock-in Thermography*. Springer, New York.

Ghiglia, D. C. and Pritt, M. D. (1998). *Two Dimensional Phase Unwrapping : Theory, Algorithm and Software*. Wiley, New York.

Kay, S. M. (1993). *Fundamentals of Statistical Signal Processing: Estimation Theory*. Prentice Hall, Englewood Cliffs.

Lugin, S. (2008). *Pulsed Thermography*. VDM Verlag, New York.

Perez, L. and Autrique, L. (2009). Robust determination of thermal diffusivity values from periodic heating data. *Inverse problems*, 25:2310–2313.

Shi, Y. Q. and Sun, H. (2000). *Image and Video Compression for Multimedia Engineering*. CRC Press, New York.